Supplementary Materials for K. Burton, R.M. Simmons & J. Sleep, "Kinetics of Force Recovery Following Length Changes in Active Skinned Single Fibres from Rabbit Psoas Muscle"

Force recovery following unloaded shortening

Fibres were suddenly unloaded by length steps large enough for the fibre to go slack and shorten at maximum velocity, so that recovery started from zero force ("slack tests", Fig. S1). Sarcomere length control was not used in this protocol, because when the fibre went slack, the feedback loop became unstable. The length-change protocol was designed so that the length at which force recovery occurred was always the same. This was achieved by applying a cycle of ramp-restretch to lengthen active fibres prior to the slack test in order to compensate for the release (Fig. S1; also see Fig. S4 chart record). The rate constants of double exponential fits to slack test recovery were 2.3 s^{-1} and 7.9 s^{-1} and the amplitude of the fast component was 68% of the total. As noted previously (Brenner & Eisenberg, 1986), force recovery after shortening at low force is poorly described by a single exponential. In the records of Fig. S1, the standard deviation of the fits for single exponentials was much higher (~7 fold) than for double exponentials, and the signal-to-noise ratio (amplitude/SD of the fit) was greatly reduced (by ~85%), so that the single-double difference curves were large.

Three exponential components could be distinguished in slack test records in which the force signal-to-noise ratio was high. The rate constant of the fastest component (9.3 $\pm$ 0.6 s^{-1}, n = 18 records, 3 fibres) was similar to that of double exponential fits (Table 1). The slow component of a double exponential fit (2.3 $\pm$ 0.04 s^{-1}, Table 1) appeared to split into two components with rate constants of 3.3 $\pm$ 0.3 s^{-1} and 1.4 $\pm$ 0.3 s^{-1} (mean ratio = 2.7 $\pm$ 0.4). Similarly, recovery after ramp shortening at low force was often well described by triple exponential fits, giving rate constants of 13.9 $\pm$ 0.4 s^{-1}, 4.3 $\pm$ 0.4 s^{-1}, and 1.0 $\pm$ 0.1 s^{-1} (n = 18 records, 4 fibres). Force recovery after the largest step releases was also frequently best fitted by three exponentials. For triple exponential fits, the slowest component was also the smallest.

Force recovery does not depend on the velocity of ramp shortening when $T_i \approx 0$

Fig. S2A shows an example of a slow ramp terminated by a step release that briefly reduced T_i (shortening = 2.5-80 nm hs^{-1} at velocity = 5-6 nm hs^{-1} s^{-1}, force = 75-90%P_O). This experiment,

and three other similar experiments, showed that the rate of force recovery was increased by the step release so that it was not significantly different from the rate of recovery in phase 4 following an isometric release (Fig. S2B and Table 1). When shortening velocity was varied so that force ranged from near zero to about $0.3P_o$, and the ramp was followed by a restretch in which T_i was lowered, recovery was also independent of shortening velocity (Fig. S3, see also Fig. 6 of the main text).

Slow decline of force following restretch

There was an overshoot in recovery (Larsson *et al.*, 1993) following a large restretch (60 nm hs^{-1}) at the end of ramp shortening , and this was followed by a slow force decline that increased with the size of the stretch (Figs. 6A, S4A). When T_{min} was made extremely high (~90%P_o) by a large restretch, there was an overshoot of about 10-20% of isometric force (Figs. S4B,C) and the slow force decline could be resolved from the force rise.

For records in which the overshoot was small (~2%P_o), and the slow falling component could not be resolved explicitly, the accelerating effect of a slow falling component was assessed by calculating a record simulated from multiple exponential functions and fitting it in the same way as the data (Fig. S5A). The simulated record was composed of two rising components and one slow falling component (Fig. S5A legend) chosen to cause a moderate overshoot on recovery (~2%P_o). When the entire time course (rise and slow fall $\approx$ 7 s) of the simulated record was fitted, the correct rate constants were recovered for the two rising components and one slow falling component (Fig. S5B). However, a double exponential fit limited to the rising phase (~1.5 sec) yielded two rising components with higher rate constants (increase of ~ 0.9 s^{-1} for each, or 36% and 10% for the slow and fast components, respectively). These effects on the simulated records were similar to those observed experimentally (Figs. S5B,C). In addition, redevelopment became more single exponential in form due to the reduction in the ratio of the two apparent rate constants (Fig. S5C). These results show that if a slow falling component is not separated from the force rise by fitting a third falling exponential, the overall recovery is effectively truncated, leading to an increase in the estimates of the rate constants, particularly of the slow rising component.

One effect of the slow fall was different in the calculated and experimental records. In the calculated records, the introduction of a slow fall reduced the apparent value of A'_f, whereas

experimentally A'_f was not affected by a slow fall (Figs. S5B,C). This difference can be explained by the observation that a large stretch reduced the amplitude of the slow rise more than the fast rise, resulting in a high A'_f (Table 2, A'_f = 0.7) and thus compensating for the expected reduction.

Effects of lowering T_{min} after a large stretch at the end of ramp shortening

The effects of forcible cross-bridge detachment on recovery were assessed by lowering force immediately after large restretches (Fig. 6; cf. Fig. 5). T_{min} was lowered in two ways (Burton, 1989): in the first the motor movement was underdamped during the restretch (Fig. 6), and in the second a step release was applied 2 ms after the restretch (Burton *et al.*, 2005). The effects of the two protocols were similar: both decreased T_{min} and hence increased the magnitude of recovery. The rate constants of both a single exponential fit and the slow component of a double exponential fit were reduced as recovery increased, whereas the rate of the fast component was relatively less affected (Fig. S6A,B). The amplitudes of the two exponential components appeared to change in the same proportion with changes in recovery magnitude (fast amplitude = 55-65% total), but as discussed above (Table 2), a relatively larger effect on the slow rise is probably masked by the presence of a slow falling component (causing an overshoot in recovery, Fig. S6C).

The rate of force recovery following shortening/restretch + release was of the same order as for large isometric step releases (Table 1), and in one experiment on the same fibre, the rates were 3, 5, 10 s^{-1} for isometric steps (8-10 nm hs^{-1}) and 3-4, 6, 13 s^{-1} for restretch + step (7-11 nm hs^{-1}).

A possible non-cross-bridge contribution to the slow rising component

Striation disorder can cause a slow rise ("creep") of force that results from shortening of shorter, stronger sarcomeres against longer, weaker sarcomeres when a fibre is held isometric (Hill, 1953; Julian & Morgan, 1979; Burton *et al.*, 1989). Although this explanation for the slow rising component cannot be completely excluded, several observations argue against it being the sole cause: 1) the slow component was present at short sarcomere lengths where the force-length relationship is stable, 2) it was observed when sarcomere length control was used, 3) it constitutes 40-50% of total force recovery, and 4) the slow rise was not noticeably increased by development of striation disorder during long activations.

Temperature dependence of force recovery

The rate of recovery increased with temperature (Fig S7A,B), as did the proportion of recovery contributed by the fast component (Fig. S7C). Results obtained in experiments done under PM and SL control were similar. The Q10's of the fitted rate constants of the fast and slow components were, respectively, 4.5-5 and 2.2-2.5 (activation energies of 114 and 57 kJ mol^{-1} obtained from linear regression to Arrhenius plots (Fig. S7B) over a temperature range of 4-9°C, correlation coefficients = 0.90 & 0.91). The Q10 for a single exponential was even higher than for the fast component, about 6.6 (activation energy of 121 kJ mol^{-1}, correlation coefficient = 0.99 over 1-9°C), owing to the greater temperature sensitivity of the magnitude of the fast component compared to the slow component.

The slow falling component, indicated by an overshoot in force recovery, could not be separated from the force rise in these records and probably caused an overestimate in the fitted rate constants. This error is expected to increase at lower temperature owing to a progressive reduction in the magnitude of the force rise relative to the overshoot, which like T_{min} is nearly independent of temperature (Fig. 7). Thus the difference between the actual rates at 4°C and 9°C is almost certainly greater than that measured. For example, at 0°C a shortening step which brought T_{min} to zero caused the apparent rate constant of a single exponential to decrease from 2.7 to 1 s^{-1}, and the slow rising component had a rate of only 0.8 s^{-1} compared to the expected value of 2 s^{-1} based on the Q10 obtained from recovery at 4-9°C (the rate of the slow component could not be obtained directly owing to the very small recovery following a restretch at 0°C (Figs. 7A, B)). When the rate constant of the slow rise at 5°C was corrected for the slow fall, it was reduced from 3.2 s^{-1} (overshoot present, Fig. S7A) to 2.3 s^{-1} (no overshoot; see Fig. S4). The Q10 calculated from the difference of this lower value and the measured rate constant at 10°C (4.5 s^{-1}, Fig. S7A) is ~3.8 rather than 2.5. The estimate of ~3.8 is an upper limit since at 10°C the slow fall is a much smaller proportion of recovery than at 5°C, requiring a smaller correction.

Fig. S8 shows Arrhenius plots of rate constants of force transients elicited by various interventions over a range of temperatures, including the ramp-restretch protocol presented here, pressure jump (Fortune *et al.*, 1994), step stretch (Ranatunga *et al.*, 2002), temperature jump (Bershitsky & Tsaturyan, 1992; Davis & Rodgers, 1995), sinusoidal analysis (Zhao & Kawai, 1994) and caged phosphate (Dantzig *et al.*, 1992; Walker *et al.*, 1992). These rate constants are similar over a large range of temperatures with Q10 = 4-5.

REFERENCES - Supplementary (see main text for others)

Burton K, Zagotta WN & Baskin RJ (1989). Sarcomere length behaviour along single frog muscle fibres at different lengths during isometric tetani. *J Muscle Res Cell Motil* **10**, 67-84.

Julian FJ & Morgan DL (1979). Intersarcomere dynamics during fixed-end tetanic contractions of frog muscle fibres. *J Physiol* **293**, 365-378.

FIGURE LEGENDS

Figure S1. Force recovery following unloaded shortening

The slack test protocol was used for four magnitudes of release. Curves as in Fig. 2A. Force recovery was not significantly dependent on release size as long as the final length was constant, so larger releases began at progressively longer lengths as shown in the graphs of fibre and sarcomere length. All of the records were obtained in a single activation under PM control (see Methods). A small length overshoot and release were present on the prestretch so that force recovery began at a reduced level (see Fig. 6). A small undershoot in the sarcomere length signal during unloaded shortening resulted from the fibre having gone slack, thus distorting the diffraction signal. Single and double exponentials were fit to recovery following the slack test (release = 5% L_O):
k_{r1} = 6.3 s^{-1}, k_{rs} = 3.8 s^{-1}, k_{rf} = 11 s^{-1}, and A'_f = 0.59 for the restretch, and for the slack test, k_{r1} = 5.6 s^{-1}, k_{rs} = 2.6 s^{-1}, k_{rf} = 8.4 s^{-1}, and A'_f = 0.66. Fibre cross section (CS) = $4x10^3$ μm^2, length = 2.53 mm.

Figure S2. Ramp shortening terminated by step release

***A*,** length and force records for 73 nm hs^{-1} shortening at low velocity (0.005 μm hs^{-1} s^{-1}, 0.0043 L_O s^{-1}) and high force, terminated by a step release of 6.8 nm hs^{-1}. The record begins near the end of the shortening ramp. The exponential fits, residuals, and differences between the single and double exponential fits are shown as in Fig. 2A of the main text. k_{r1} = 3.6 s^{-1}, k_{rs} = 2.0 s^{-1}, k_{rf} = 9.8 s^{-1}, and A'_f = 0.56. CS = $4.0x10^3$ μm^2, length = 2.1 mm. Sarcomere length control. ***B*,** comparison of single and double exponential fits to force recovery from near zero in one fibre following ramp/release (diagonally hatched bars) as in (*A*) or isometric step release (cross-hatched bars). n = 10 records for ramp/releases and n = 5 for isometric step releases.

Figure S3. Ramp shortening at various loads with ringing on the restretch

Shortening ramps are shown at velocities of 0.09-0.7 L_o s^{-1} (PM control). The ramps were terminated by a restretch to the original length; ringing on the restretch (4.4%L_o over ~1.2 ms) brought force to a low level at the beginning of recovery. In the records shown, data acquisition was too slow (4 ms per point) to fully sample the ringing on the restretch or the corresponding brief force response (upward and downward spikes on the time scale shown). Exponential fits and residuals are shown as in Fig. 2A of the main text. Fits to recovery after shortening at the highest force (lowest velocity, 0.09 L_o s^{-1}), yielded

k_{r1} = 4.0 s^{-1}, k_{rs} = 2.1 s^{-1}, k_{rf} = 9.0 s^{-1}, and A'_f = 0.58, and at the lowest force (0.7 L_o s^{-1}), k_{r1} = 3.9 s^{-1}, k_{rs} = 2.0 s^{-1}, k_{rf} = 8.8 s^{-1}, and A'_f = 0.63. For all the records, k_{r1} = 3.8 $\pm$ 0.05 s^{-1}, range = 3.6-4.0 s^{-1}; k_{rs} = 2.0 $\pm$ 0.02 s^{-1}, range = 1.9-2.1 s^{-1}; k_{rf} = 8.9 $\pm$ 0.08 s^{-1}, range = 8.6-9.2 s^{-1}, n = 7 records. CS = 4.6x10^3 μm^2, length = 2.45 mm.

Figure S4. Slow fall of force following ramp-restretch

A, plot of the overshoot in force recovery resulting from the presence of a slow falling component *vs*. the size of a stretch applied at the end of high velocity shortening. The overshoot is defined as the value approached at infinite time by a double exponential fit up to the plateau of recovery, divided by the steady isometric force prior to ramp shortening. Number of records as in Fig. 5B.

B, Example of a force record with an extremely high T_{min} and large overshoot that was sampled well beyond the plateau of recovery. A single exponential (**+**) was fitted to the plateau of recovery, and double (×) and triple (□) exponentials were fitted over the full time course. For the single exponential, k_{r1} = 6 s^{-1}, and for the double exponential with one rising and one falling component, k_{r1} = 5.1 s^{-1} and k_s = 0.23 s^{-1}, where k_s is the rate constant of the slow fall, and for the triple exponential with two rising and one falling component, k_{rs} = 2.5 s^{-1}, k_{rf} = 7.0 s^{-1}, A'_f = 0.67, and k_s = 0.34 s^{-1}.

C, chart record showing overshoot of force recovery on a slow time base. The periodic downward deflections at 5.5 sec intervals result from ramp-restretch cycles used to maintain striation order (see Methods). An overshoot in force recovery, large in this example to illustrate the behaviour, was most easily observed when the time between cycles was increased (up to 25 sec in this example). The double vertical deflections represent slack tests, and the final downward deflection shows relaxation. CS = 6.43x10^3 μm^2, length = 2 mm, sarcomere length = 2.33 μm.

Figure S5. Exponential fits to calculated records containing a falling component

A, multiple exponential functions calculated to appear similar to experimental data with or without a small overshoot in recovery. The rate constants and amplitudes of the calculated curves were, respectively, k_S = 0.5 s^{-1}, k_{rS} = 2.5 s^{-1}, k_{rf} = 8 s^{-1}, with amplitudes = 0.06, -0.25, and -0.31 (units of "P_O", negative for the rising components); A'_f = 0.55. k_{rS} and k_{rf} are defined in Fig. 2A. The slow falling component (k_S) produced a 2.3% overshoot. The upper graph shows the calculated traces (solid lines) over periods of two seconds (main graph) and 7 seconds (inset) with and without a falling component (upper and lower traces, respectively). The dashed lines show single exponential fits to the traces. The lower graph shows residuals of the single exponential fits to the traces with 0% and 2.3% overshoot (short and long dashed lines, respectively), as well as a double exponential fit to the 2.3% trace (2 rising components, solid line). A falling component reduced the residuals of a single exponential fit, making the rising phase more nearly single exponential.
B, comparison of fits to the rising phases of calculated traces and experimental traces with and without a small overshoot in recovery. The fits to the calculated traces (solid bars) are discussed above in (*A*) (open bars = 0% overshoot, and closed bars = 2.3% overshoot produced by the slow falling component). The experimental values (diagonally hatched bars) are taken from a weighted average of the results in SL and PM control described in Fig. S6 for recovery from near zero with no overshoot (wide hatch, *n* = 43 records) and recovery from 40-50%P_O with a 2.3%P_O overshoot (narrow hatch, *n* = 97).
C, Bottom graph: as in (*B*), but showing ratios of fit parameters from traces with and without the small overshoot for calculated (vertically hatched bars) and experimental (gray bars) records.

Figure S6. Underdamped restretch or restretch + step release

*G*raphs showing the relationship between observed magnitude of recovery (defined in Fig. 5*C*) and the rates of force recovery (*A,B*) and fitted offset *(C)*. Data taken from experiments in which recovery magnitude was varied using ringing (Fig. 6*A*) or step releases after the restretch.
***A*,** rate constants are shown for single exponential fits (k_{r1}, solid lines, (■,□)) and double exponential fits (broken lines) for the slow (k_{rS}, (▲,△)) and fast (k_{rf}, (▼,▽)) rising components. Open symbols refer to SL-control data and closed symbols to PM-control data. The data were acquired from 34 fibres, and for single exponential fits in PM and SL control, *n* = 16-77 and 4-23 records, respectively, for each magnitude of recovery, and for double exponential fits, *n* = 30-78

and 4-43 records.

***B*,** as in (*A*), but the rate constants for each fibre were normalized to those obtained at recovery magnitude = 60%P_O, and then averaged among fibres to show their relative dependence on recovery magnitude. SL and PM control data were averaged together as in Fig. 2B.

***C*,** "Overshoot" = offset of the exponential fit relative to that at 60% recovery within each fibre, at which the offset was ~P_O (see Fig. S4A). Dashed and solid lines – SL and PM control.

Figure S7. Force recovery *vs.* temperature

A, rate constants for the single (⊡), slow (△), and fast (▽) rising components *vs.* temperature over 1–9°C. For the single exponential fits, *n* (sets of 2-3 repeats at each temperature) = 4 at 1-8°C and 2 at 9°C, and for the double exponential fits, *n* = 1, 2, 4, 3, & 2 at 1, 2-4, 5-7, 8, & 9°C, respectively. *n* was smaller at low temperature owing to the progressively smaller magnitude of recovery, which reduced the reliability of double exponential fits. At high temperature, sarcomere disorder increased and thus reduced the quality of the data acquired in sarcomere length control. The results are taken equally from SL and PM control data.

B, Arrhenius plots of the rate constants shown in (*C*). The lines show linear regression through the points in the graph, with each value weighted by *n*. Q10's = 4.5-5.0 and 2.2-2.5 for the rate constants of the fast and slow rising components, respectively (calculated from linear regression over a temperature range of 4-9°C), and ~6.6 over 1-9°C for single exponentials. R is the gas constant and T is absolute temperature.

C, amplitude of the fast component (A_f) as a proportion of total recovery ($A_f/A_T = A'_f$) (⊙) or relative to its value at 5°C (◇).

Figure S8. Temperature dependence of related force transients

Arrhenius plot of the rate constant of the fast component of force recovery elicited by ramp-restretch (□) compared to those of force transients elicited by other perturbations, including pressure release ("phase 2" of Fortune *et al.*, 1994 (▲)), caged phosphate (k_{pi} of Dantzig, *et al.*, 1992 (◇) and Walker *et al.*, 1992 (△)), sinusoidal analysis ("process b" of Zhao & Kawai, 1994 (◯)), temperature jump ("phase 2" of Bershitsky & Tsaturyan, 1992 (■) and τ_{neg}^{-1} of Davis & Rodgers, 1995 (▼), and step stretch ("phase 2b" of Ranatunga *et al.*, 2002 (●)). The lines show linear regression through the points in the graph for the four data sets that have values at more than one temperature. Some values have been estimated from Q10s taken from the data, and these are

marked with a (**+**). The rate constant of phase 2 of the pressure release response is shown at 12°C (28 s^{-1}, Fortune *et al.*, 1994); the temperature-dependence was reported separately (Fortune, 1990), with the Q10s of their phases 2 and 3 ≈ 4.5-5 and ≈2, respectively. The values shown in the graph refer to experiments at low phosphate concentration (~1 mM). The published temperature-jump data of Davis & Rodgers (1995, τ_{neg}^{-1}) were obtained at 15 mM phosphate, and are similar to the rate of force recovery elicited by ramp-restretch at that phosphate concentration (Burton *et al.*, 2005), ~1.9-fold higher than reported here. On the assumption that the two types of force response share the same phosphate-dependence, their data have been reduced by the same factor to give the data points shown in the graph. The rate of force recovery following ramp-restretch at 20°C was obtained from fibres rapidly activated by release of ATP from a caged precursor (Sleep *et al.*, 2005).

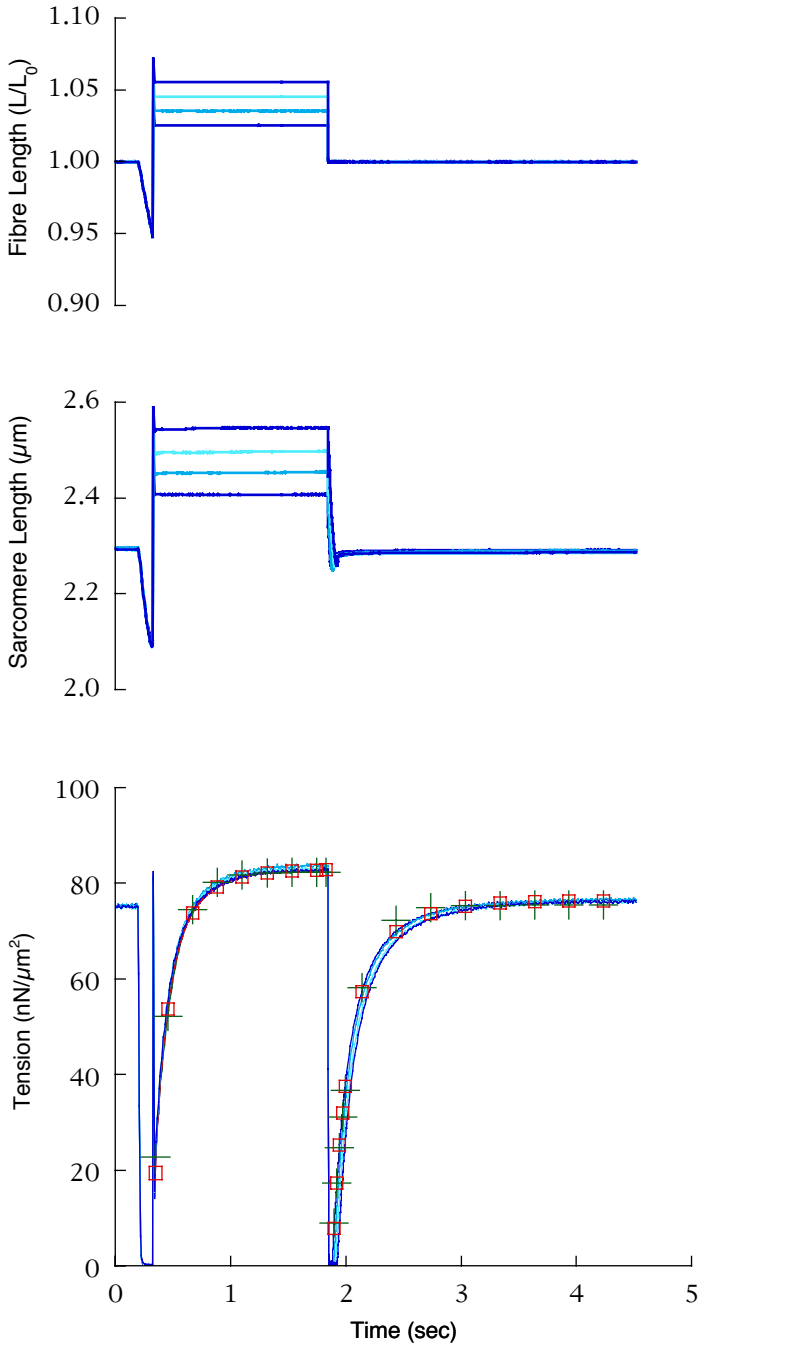
Fibre Length (L/L0)
1.10
1.05
1.00
0.95
0.90
Sarcomere Length (μm)
2.6
2.4
2.2
2.0
Tension (nN/μm2)
100
80
60
40
20
0
0
1
2
3
4
5
Time (sec)
Residual
0.04
0.02
0.00
-0.02
-0.04
5%
Fits
Double
Single
Single-Double
0.04
0.02
0.00
-0.02
-0.04

Fig. S1

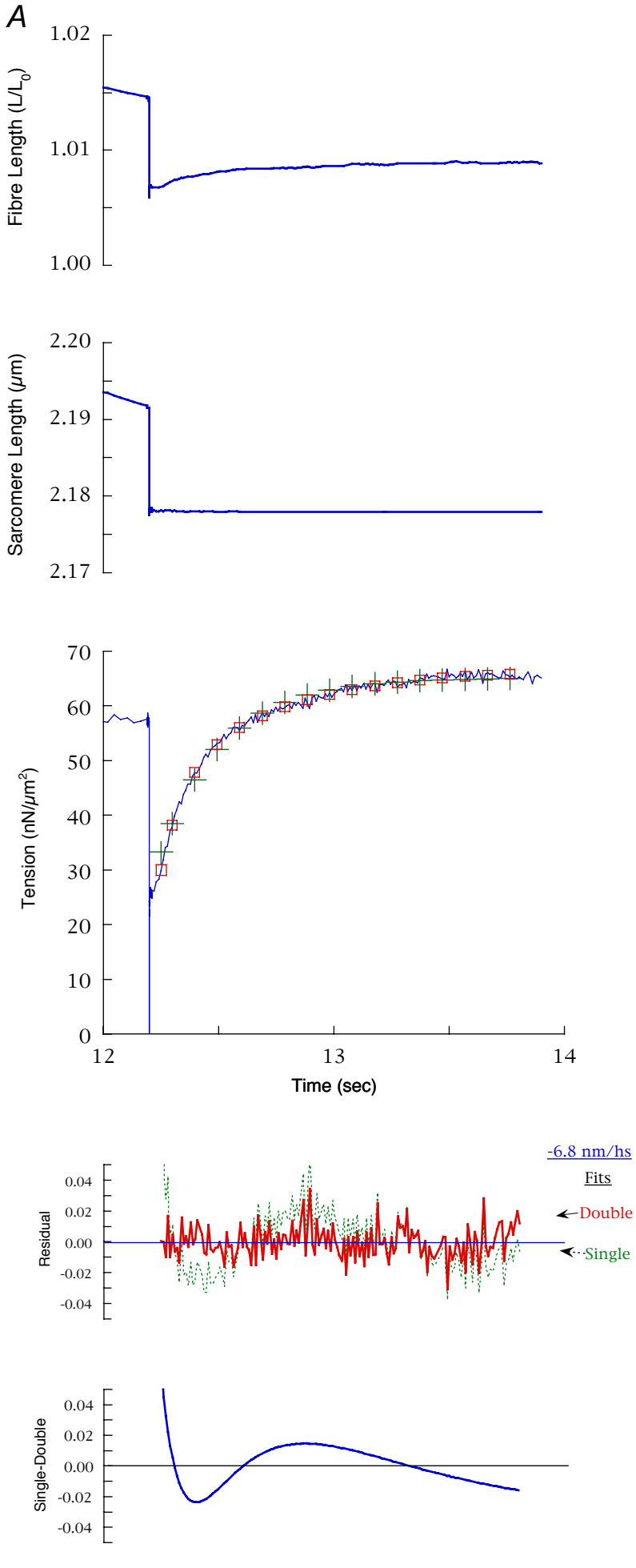
A
1.02
1.01
1.00
Fibre Length (L/L0)
2.20
2.19
2.18
2.17
Sarcomere Length (μm)
70
60
50
40
30
20
10
0
12
13
14
Tension (nN/μm2)
Time (sec)
-6.8 nm/hs
Fits
Double
Single
0.04
0.02
0.00
-0.02
-0.04
Residual
0.04
0.02
0.00
-0.02
-0.04
Single-Double

Fig. S2

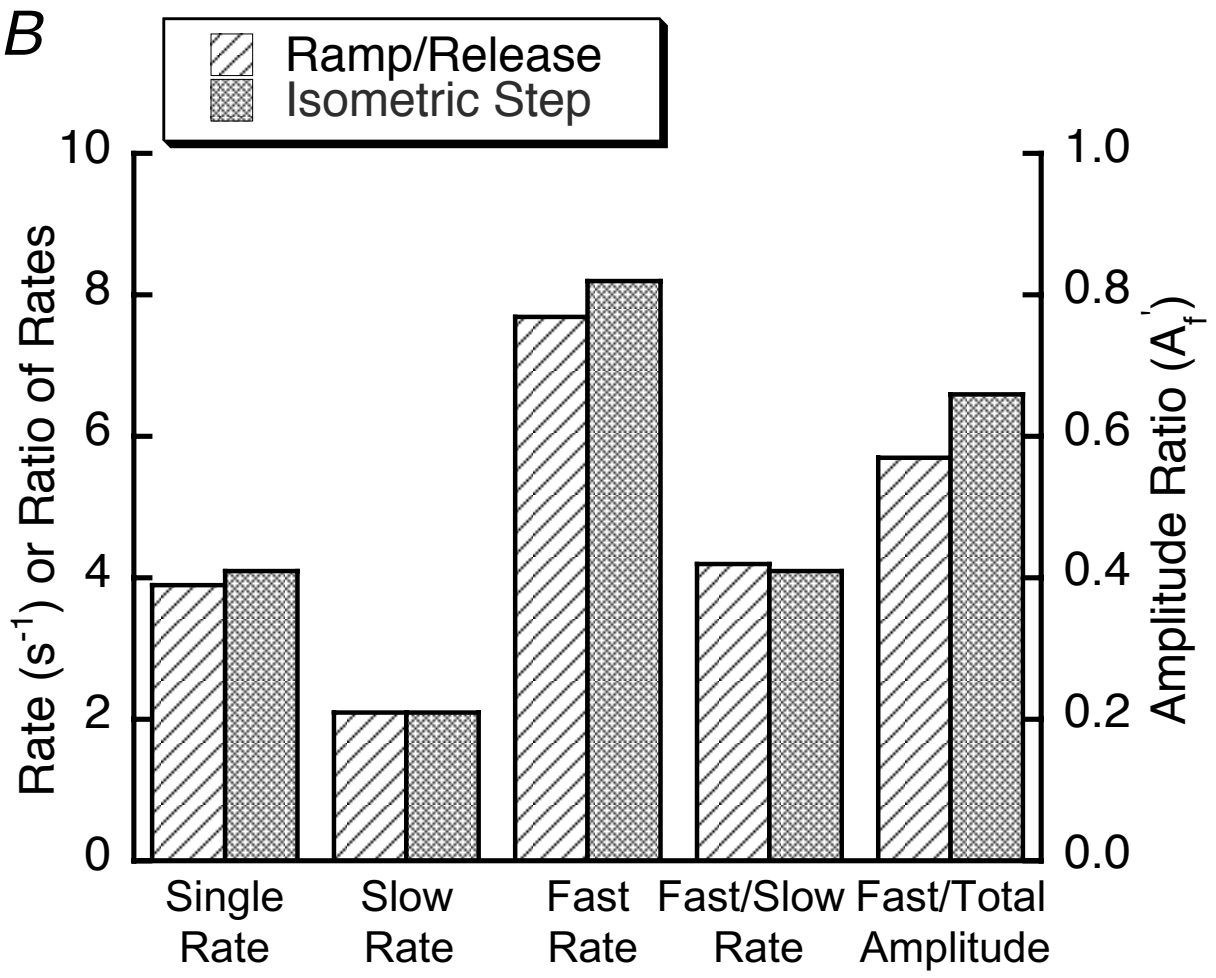
B
Ramp/Release
Isometric Step
Rate (s-1) or Ratio of Rates
Amplitude Ratio (Af')
10
8
6
4
2
0
1.0
0.8
0.6
0.4
0.2
0.0
Single Rate
Slow Rate
Fast Rate
Fast/Slow Rate
Fast/Total Amplitude

Fig. S2

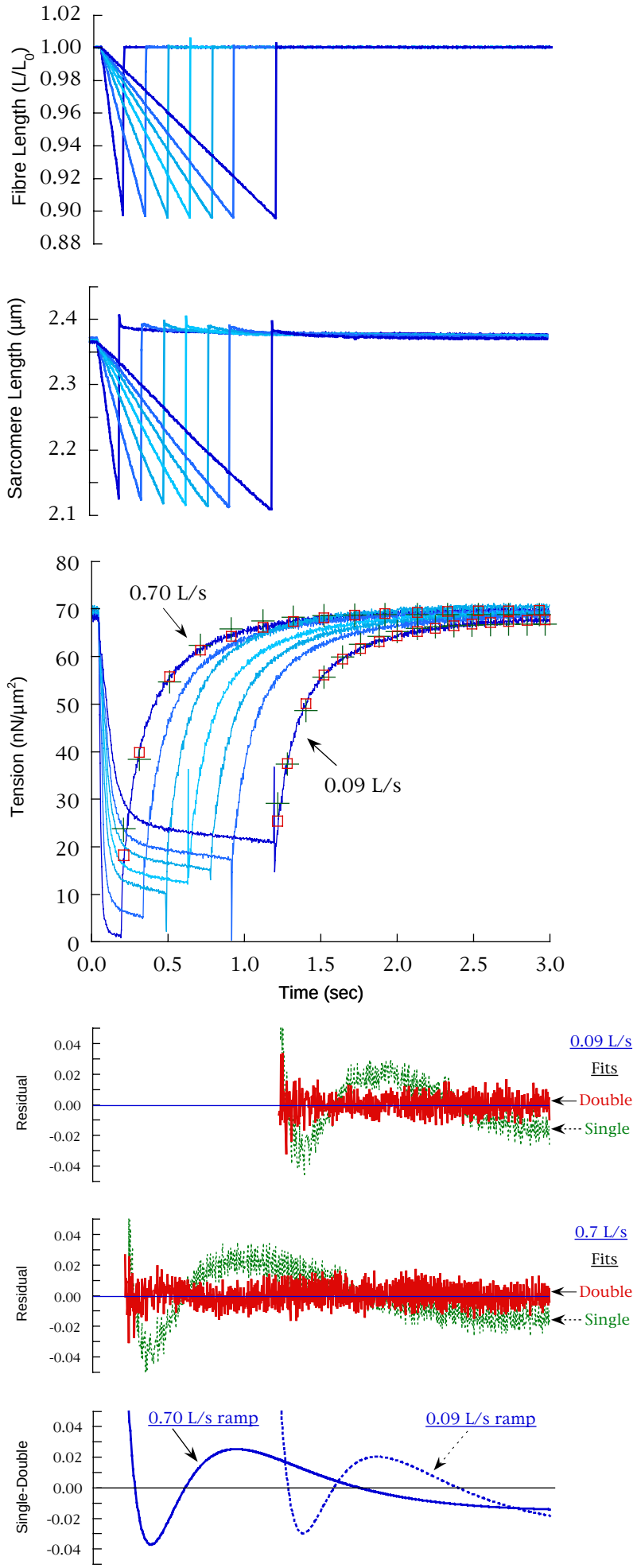
Fibre Length (L/L0)
1.02
1.00
0.98
0.96
0.94
0.92
0.90
0.88
Sarcomere Length (µm)
2.4
2.3
2.2
2.1
Tension (nN/µm2)
80
70
60
50
40
30
20
10
0
0.70 L/s
0.09 L/s
0.0
0.5
1.0
1.5
2.0
2.5
3.0
Time (sec)
Residual
0.04
0.02
0.00
-0.02
-0.04
0.09 L/s
Fits
Double
Single
Residual
0.7 L/s
Fits
Double
Single
Single-Double
0.70 L/s ramp
0.09 L/s ramp

Fig. S3

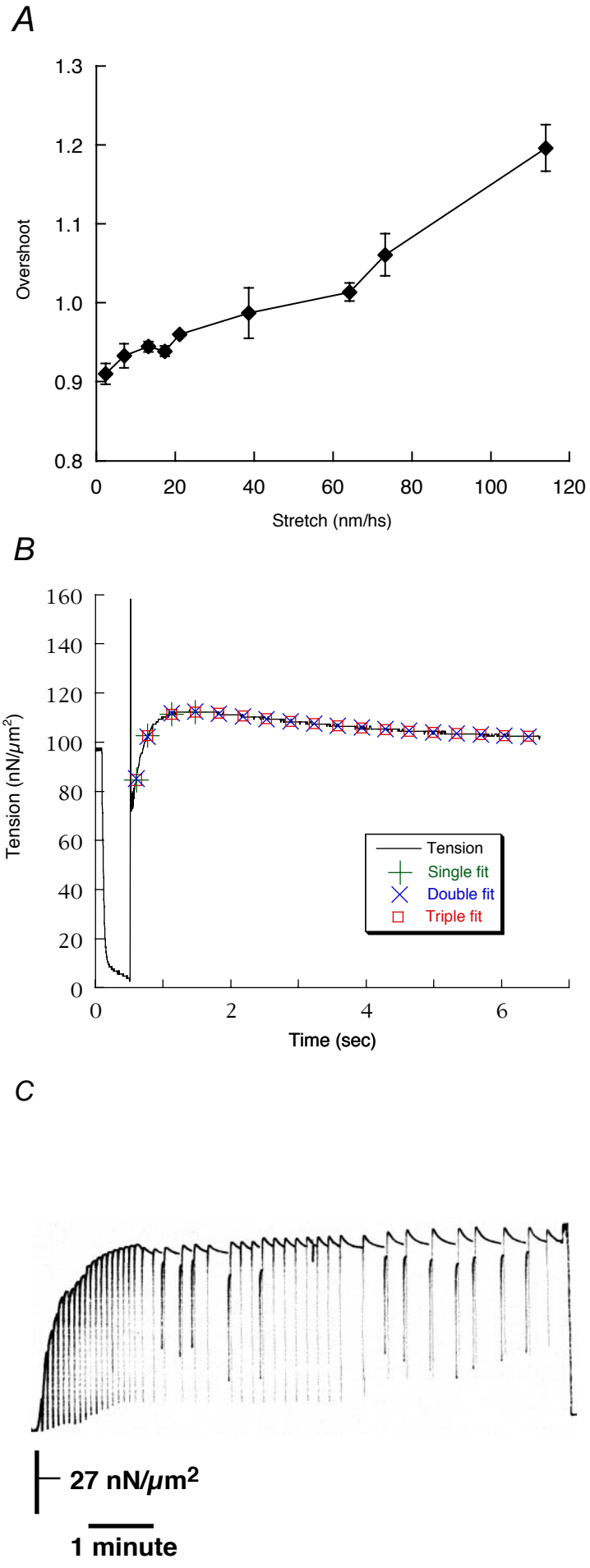
A
1.3
1.2
1.1
1.0
0.9
0.8
Overshoot
0
20
40
60
80
100
120
Stretch (nm/hs)
B
160
140
120
100
80
60
40
20
0
Tension (nN/μm²)
0
2
4
6
Time (sec)
Tension
Single fit
Double fit
Triple fit
C
27 nN/μm²
1 minute

Fig. S4

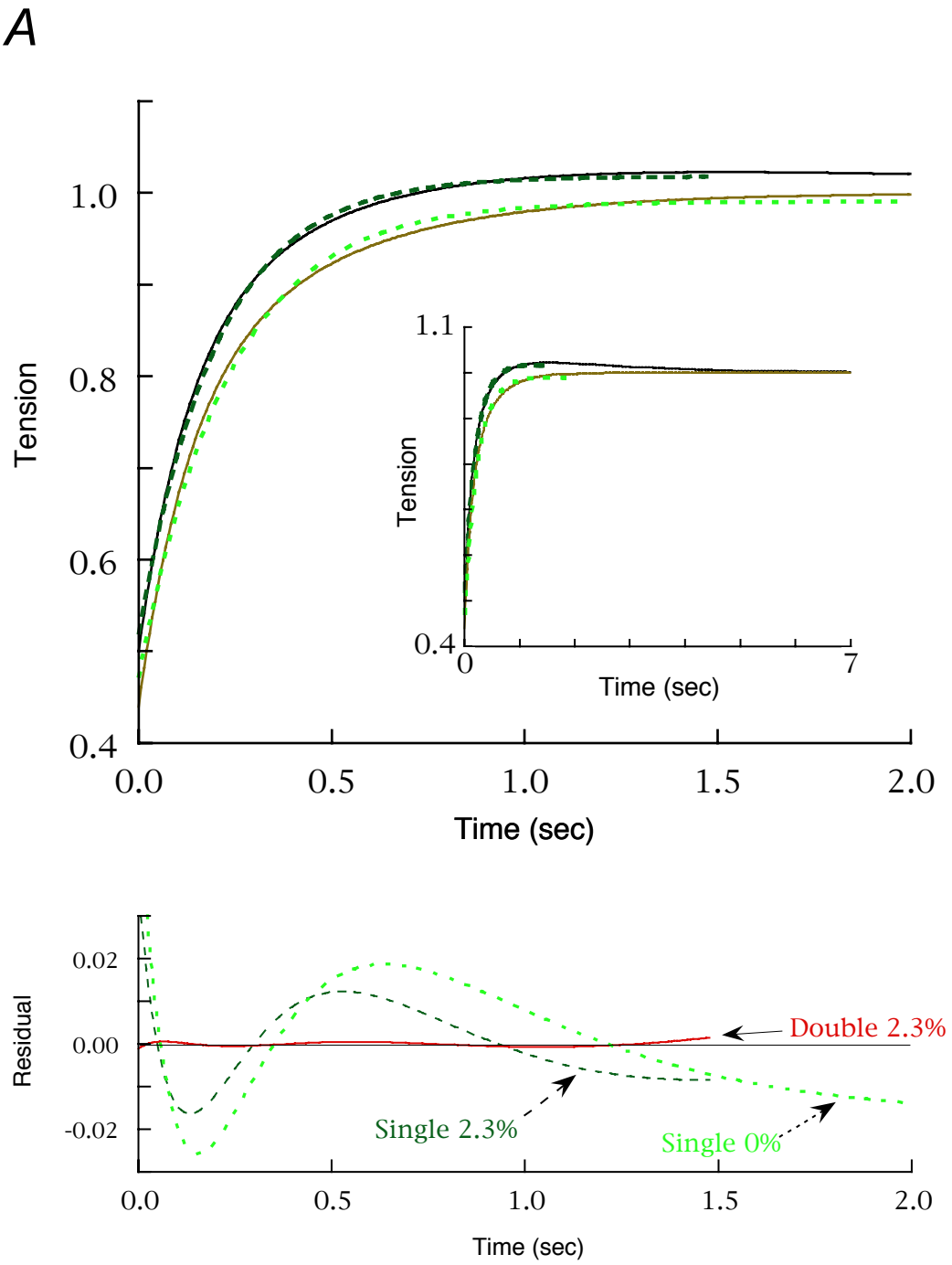
A
Tension
1.0
0.8
0.6
0.4
0.0
0.5
1.0
1.5
2.0
Time (sec)
1.1
Tension
0.4
0
7
Time (sec)
Residual
0.02
0.00
-0.02
Double 2.3%
Single 2.3%
Single 0%
0.0
0.5
1.0
1.5
2.0
Time (sec)

Fig. S5

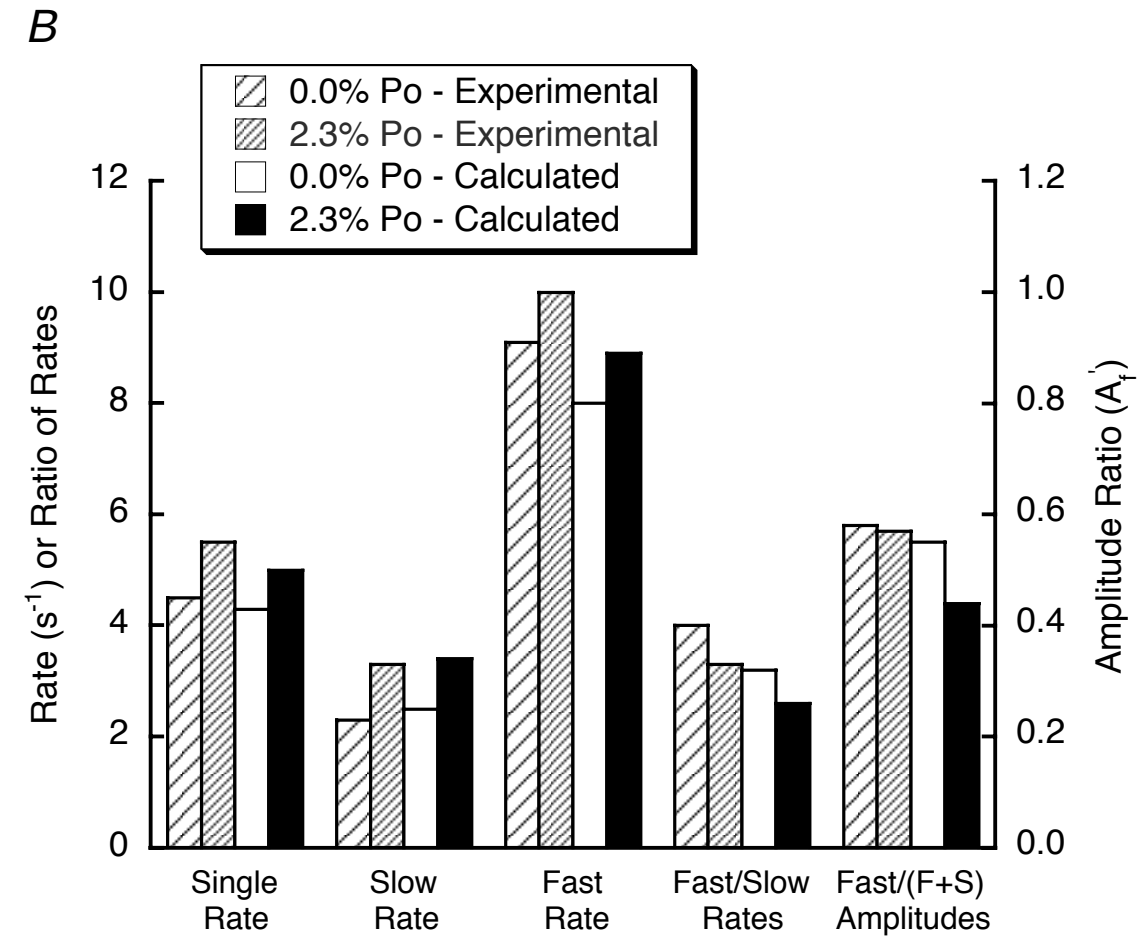
B
0.0% Po - Experimental
2.3% Po - Experimental
0.0% Po - Calculated
2.3% Po - Calculated
Rate (s-1) or Ratio of Rates
Amplitude Ratio (A'f)
0
2
4
6
8
10
12
0.0
0.2
0.4
0.6
0.8
1.0
1.2
Single Rate
Slow Rate
Fast Rate
Fast/Slow Rates
Fast/(F+S) Amplitudes

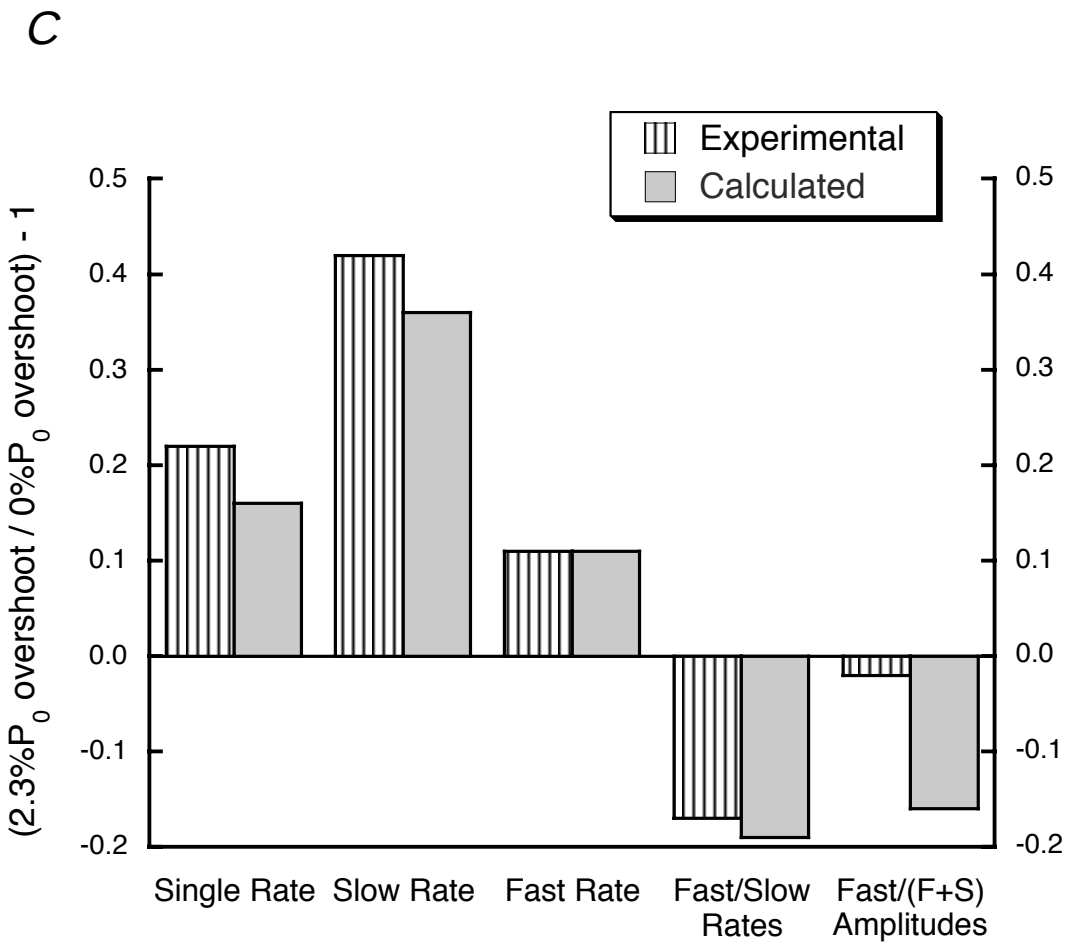
C
Experimental
Calculated
(2.3%P0 overshoot / 0%P0 overshoot) - 1
0.5
0.4
0.3
0.2
0.1
0.0
-0.1
-0.2
Single Rate
Slow Rate
Fast Rate
Fast/Slow Rates
Fast/(F+S) Amplitudes

Fig. S5

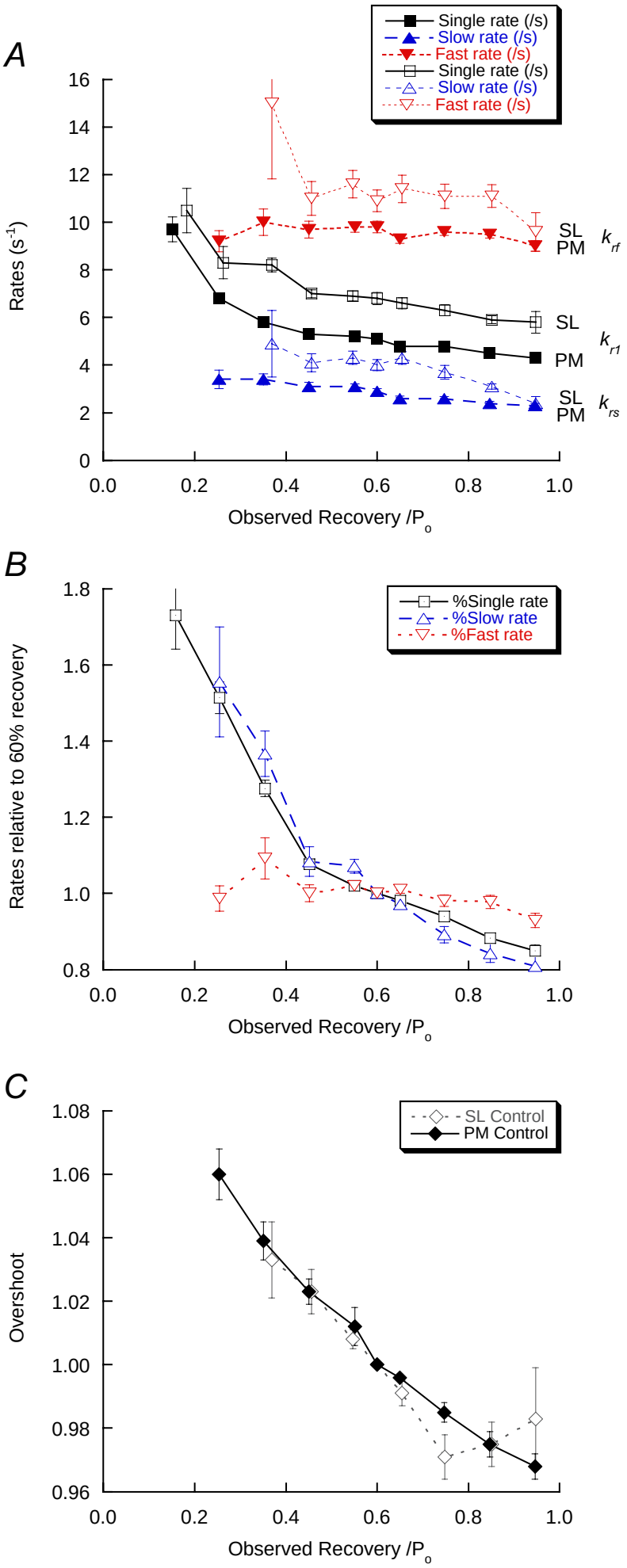
A
Single rate (/s)
Slow rate (/s)
Fast rate (/s)
Single rate (/s)
Slow rate (/s)
Fast rate (/s)
Rates (s-1)
SL
PM
krf
SL
PM
kr1
SL
PM
krs
Observed Recovery /Po
B
%Single rate
%Slow rate
%Fast rate
Rates relative to 60% recovery
Observed Recovery /Po
C
SL Control
PM Control
Overshoot
Observed Recovery /Po

Fig. S6

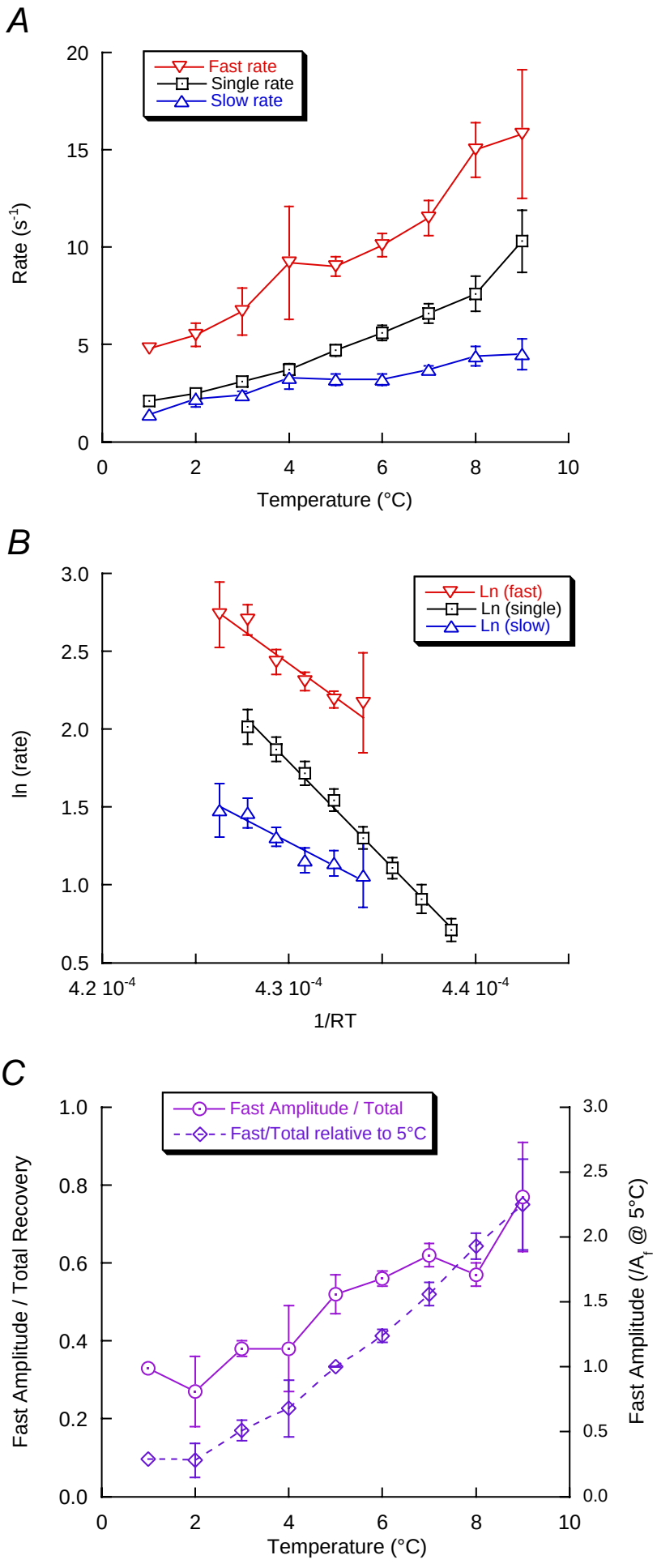
A
Fast rate
Single rate
Slow rate
Rate (s-1)
Temperature (°C)
B
Ln (fast)
Ln (single)
Ln (slow)
ln (rate)
1/RT
C
Fast Amplitude / Total
Fast/Total relative to 5°C
Fast Amplitude / Total Recovery
Fast Amplitude (/Af @ 5°C)
Temperature (°C)

Fig. S7

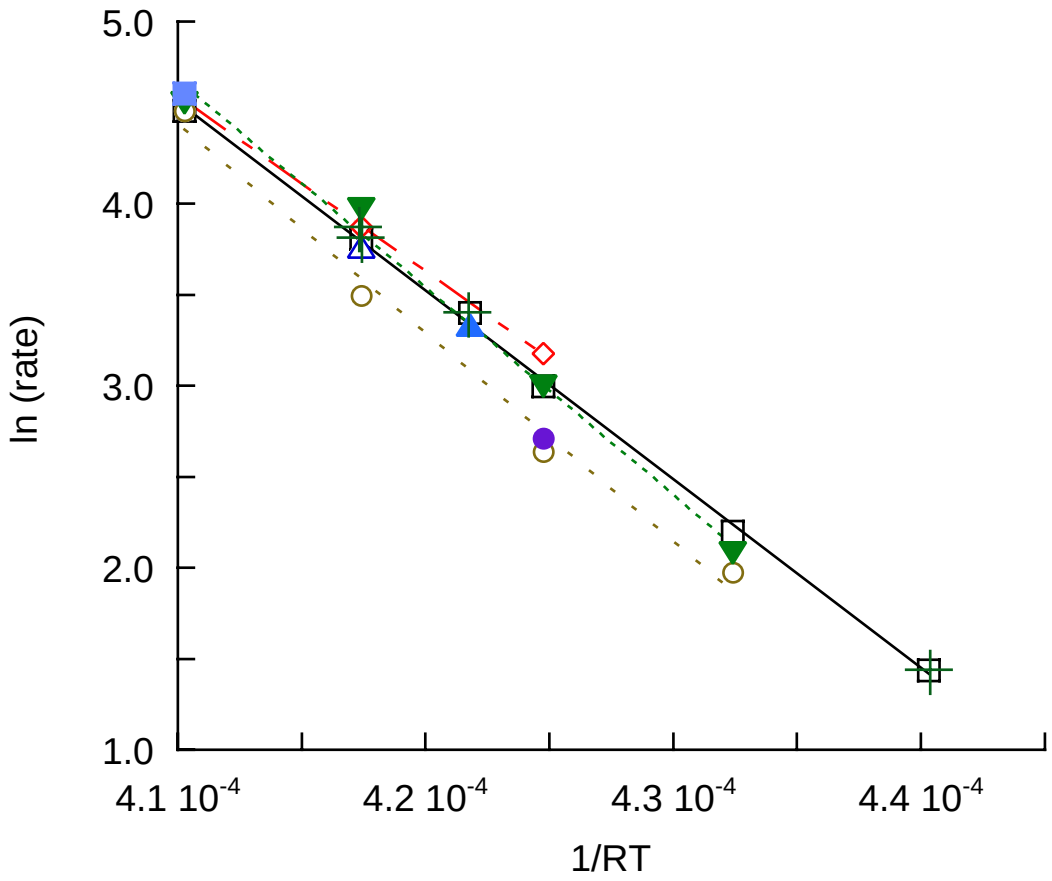

Fig. S8